Frontiers of Physics
https://doi.org/10.1007/s11467-021-1093-6
Front. Phys.
17(1), 13502 (2022)

RESEARCH ARTICLE

Enhanced photogalvanic effect in the two-dimensional $MgCl_2/ZnBr_2$ vertical heterojunction by inhomogenous tensile stress

Liyu Qian, Juan Zhao, Yiqun Xie†

Department of Physics, Shanghai Normal University, 100 Guilin Road, Shanghai 200234, China
Corresponding author. E-mail: †yqxie@shnu.edu.cn
Received February 22, 2021; accepted June 7, 2021

The photogalvanic effect (PGE) occurring in noncentrosymmetric materials enables the generation of a dc photocurrent at zero bias with a high polarization sensitivity, which makes it very attractive in photodetection. However, the magnitude of the PGE photocurrent is usually small, leading to a low photoresponsivity, and therefore hampers its practical application in photodetection. Here, we propose an approach to largely enhancing the PGE photocurrent by applying an inhomogenous mechanical stretch, based on quantum transport simulations. We model a two-dimensional photodetector consisting of the wide-bandgap $MgCl_2/ZnBr_2$ vertical van der Waals heterojunction with the noncentrosymmetric C_{3v} symmetry. Polarization-sensitive PGE photocurrent is generated under the vertical illumination of linearly polarized light. By applying inhomogenous mechanical stretch on the lattice, the photocurrent can be largely increased by up to 3 orders of magnitude due to the significantly increased device asymmetry. Our results propose an effective way to enhance the PGE by inhomogenous mechanical strain, showing the potential of the $MgCl_2/ZnBr_2$ vertical heterojunction in the low-power UV photodetection.

Keywords photogalvanic effect, mechanical stretch, polarization-sensitive, vertical heterojunction, ultraviolet photodetection

1 Introduction

Ultraviolet (UV) photodetectors (PDs) have been widely utilized in military and civilian fields, such as missile detection, environmental monitoring, and space optical communications [1–3]. Robust photoresponsivity, high polarization sensitivity, low-energy power consumption, ultra-small size and good flexibility are important figure of merits for the UV photodetections. In recent years, UV-PDs based on two-dimensional (2D) semiconductors have shown great potential to fulfill these demands. There has been considerable research on UV-PDs based on the 2D wide bandgap (2D-WBG) semiconductors, such as MgO with an energy gap (Eg) of 7.3 eV [4] few-layered h-BN [5] and $FePS_3$ [6]. Outstanding performances have been achieved via such 2D-WBG UV-PDs. For example, the graphene/ZnS/4H-SiC photodetector has demonstrated an ultrafast photoresponse to 250 nm light with a 28 ms rise time [7].

Various mechanisms are responsible for the generation of the photocurrent in these photodetectors, which include the photovoltaic effect, photogating, photoconducting, as well as photothermal effects. Of particular importance is the photogalvanic effect (PGE) that occurs in materials without the space inversion symmetry under the illumination of polarized light [8–15]. The PGE is able to generate a dc photocurrent that is highly polarization sensitive, without the need for any external electric fields or a pn-junction. Therefore, the PGE is a perfect mechanism for the self-powered and polarization sensitive UV photodetection with a low dark current. In our previous work, we have proposed the UV photodetection based on the PGE by using the photodetector consisting of the wide-bandgap 2D materials and their heterostructures [16]. A recent experiment has also demonstrated that the PGE is an effective mechanism for the UV photodetection with a high polarization sensitivity and low dark current [17].

However, the magnitude of the PGE photocurrent is usually small, which leads to a relatively low photoresponsivity typically of mA/W. Therefore, it is of practical importance to find a mechanism to enhance the magnitude of the PGE photocurrent. Several recent experiments have suggested that the PGE photocurrent can be largely enhanced under mechanical strains [18–20]. It has been shown that, by applying an appropriate mechanical stress

* arXiv: 2106.13526. This article can also be found at http://journal.hep.com.cn/fop/EN/10.1007/s11467-021-1093-6.

© Higher Education Press 2022

gradient on the $SrTiO_3$ single crystal, the PGE photocurrent can be enhanced by orders of magnitude [21], which is known as the flexophotovoltaic efect, though the controversy was raised regarding on the underlying mechanism [22]. Direct experimental evidence for the efective enhancement of the PGE by mechanical strain has recently been achieved in the Fe-doped $LiNbO_3$ single crystal, in which the photocurrent was increased by 75% even under a tiny uniaxial compressive stress (0.005%) on the lattice [23]. Motivated by these experimental findings, we have investigated the influence of uniform mechanical tensile stress on the PGE for a phosphonene photodetector by using quantum transport simulations, and proposed that the large enhancement of the PGE photocurrent is mainly due to the strain-increased device asymmetry [24].

In this work, using quantum transport simulations, we present a theoretical study on the PGE in the photodetector based on the 2D $MgCl_2/ZnBr_2$ vertical van der Waals heterojunction (vdWH). By applying an inhomogenous mechanical tensile stress on the photodetector, the PGE photocurrent can be largely enhanced under the illumination of linearly polarized light. Our results propose an effective approach to enhancing the PGE, suggesting its promising application in the low-power UV photodetection.

2 Model and methods

The 2D monolayer $MgCl_2$ and $ZnBr_2$ have recently been predicted with a stable configuration [25]. Their primitive cells contain two haloid atoms (Cl, Br) and a metal atom (Mg, Zn), as shown in Figs. 1(a) and (b). The lattice constant is 3.645 Å and 3.761 Å for $MgCl_2$ and $ZnBr_2$, with the bandgap of 6.0 eV and 3.41 eV, respectively, according to our previous first-principle calculations [16]. Since the monolayer $MgCl_2$ and $ZnBr_2$ have a centrosymmetric D_{3d} symmetry, the PGE cannot be generated. Therefore, to obtain the PGE, we construct a vdWH using the monolayer $MgCl_2$ and $ZnBr_2$, as shown in Fig. 1. This vdWH has the noncentrosymmetric C_{3v} symmetry, and therefore the PGE can be generated under the vertical illumination of linearly polarized light.

The electronic bandstructure of the $MgCl_2/ZnBr_2$ vdWH are calculated using the Vienna Ab-initio Simulation Package (VASP) [26, 27]. The plane wave basis set with the projector augmented wave (PAW) pseudopotential is adopted. The exchange correlation potentials are approximated using the generalized gradient approximation (GGA) functional as parameterized by Perdew, Burke and Ernzerhof (PBE) functional [28]. Brillouin zone integration is performed with a 15×1×15 k-point mesh for geometry optimization and self-consistent electronic structure calculations. The kinetic energy cutoff for the plane wave basis is 500 eV. All the atoms in the unit cell are fully relaxed until the force on each atom is less than

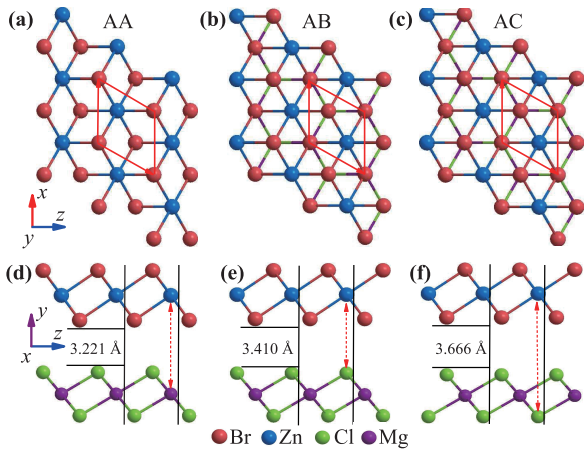

Fig. 1 Three kinds of stacking patterns of the 2D $MgCl_2/ZnBr_2$ vertical vdWH. **(a)**, **(b)** and **(c)** are top views for AA, AB and AC configurations, respectively, and **(d)**, **(e)** and **(f)** are corresponding side views. The red arrows in (a) denote the lattice constants of the primitive cell.

0.001 eV/Å and the convergence criteria for energy in the self-consistent field cycle was 10^{-6} eV. The supercell is periodic in the xz-plane and is separated by a 20 Å vacuum layer in the z-direction to avoid the interaction between the imaginary cells.

The photocurrent is calculated using the first-principles quantum transport package NanoDcal [29], where density functional theory is used combined with nonequilibrium Green's formalism (NEGF-DFT). The photocurrent is calculated based on linear response theory [30]. Specifically, for linearly polarized light, the photocurrent injecting into the left lead (electrode) can be written as [16, 31–34]

$$\begin{aligned} J_L^{(ph)} = \frac{\mathrm{i}e}{h}\int\{&\cos^2\theta \mathrm{Tr}\{\Gamma_L[G_1^{<(ph)}+f_L(G_1^{>(ph)}-G_1^{<(ph)})]\} \\ &+\sin^2\theta \mathrm{Tr}\{\Gamma_L[G_2^{<(ph)}+f_L(G_2^{>(ph)}-G_2^{<(ph)})]\} \\ &+2\sin(2\theta)\mathrm{Tr}\{\Gamma_L[G_3^{<(ph)}+f_L(G_3^{>(ph)} \\ &-G_3^{<(ph)})]\}\}\mathrm{d}E, \end{aligned}$$

where $G_{1,2,3}^{>/<(ph)}$ denotes the greater/lesser Green's functions with electron-photon interaction, which are determined by the symmetry, photon frequence and polarization vector $\boldsymbol{e}$. For linearly polarized light, the polarization vector $\boldsymbol{e} = \cos\theta\boldsymbol{e}_1 + \sin\theta\boldsymbol{e}_2$, where θ is the angle formed by the polarization direction with respect to the vector $\boldsymbol{e}_1$. The vectors $\boldsymbol{e}_1$ and $\boldsymbol{e}_2$ are set along the zigzag and armchair directions, respectively. The photocurrent can be normalized as, $I_{ph} = J_L^{(ph)}/(eI_\omega)$ which still has dimensions of area of a_0^2/photon, where a_0 is the Bohr radius. In the numerical calculations, the DZP atomic orbital basis is used to expand all the physical quantities; the exchange and correlation were treated at the level of the GGA functional as parameterized by the PBE approximation; atomic cores are determined by the standard

norm conserving nonlocal pseudopotentials, and 16×1×1 k-points are used. These calculation details are verified to obtain converged results.

According to our previous work [24], the magnitude of the PGE photocurrent is determined by the $|J_L^{(ph)}| = \Delta J = |J_+ - |J_-||$, where $J_- = \frac{ie}{h}\int_{-\infty}^{0} \mathrm{Tr}[\Gamma_L G^{>(ph)}]\mathrm{d}E < 0$ denotes the current flowing out the center region to the left lead, while $J_+ = \frac{ie}{h}\int_{0}^{+\infty} \mathrm{Tr}[\Gamma_L G^{<(ph)}]\,\mathrm{d}E > 0$ denotes the current flowing into the center region from the lead. Therefore we can define a factor A to describe the device asymmetry as

$$A = \left|\frac{J_+ - |J_-|}{J_+}\right| \tag{1}$$

For the device with the space inversion symmetry the current flowing into the center region equals that out of the center region, that is, there is no net current flowing through the device. In this case, $J_+ = |J_-|$, so that $J_L^{(ph)} = 0$, and A=0. For the device without the inversion symmetry, there is a net photocurrent and A is nonzero. The magnitude of the photocurrent can then be rewritten as

$$|J_L^{(ph)}| = AJ_+. \tag{2}$$

In the below, we will show that the device asymmetry plays a dominant role in enhancing the photocurrent under inhomogenous mechanical stress.

3 Results and discussion

We consider three configurations of the 2D $MgCl_2/ZnBr_2$ vertical vdWHs, namely, AA, AB and AC, as shown in Fig. 1. The lattice constant of the $ZnBr_2$ (3.761 Å) is used for the heterostructure, which means a 3.18% stretch in the lattice of the $MgCl_2$. For the AA structure, the Zn atoms in the top layer of $ZnBr_2$ lie directly above the Mg atoms in the bottom layer of $MgCl_2$, as shown in Fig. 1(a). For the AB structure, the Zn atoms of the top $ZnBr_2$ layer lie directly above the Br atoms in the top-sublayer of the $MgCl_2$ [Fig. 1(b)]. For the AC structure, Zn atoms of the top $ZnBr_2$ layer are directly above the Br atoms of the bottom $MgCl_2$ sublayer [Fig. 1(c)]. We calculate the binding energy of the three heterojunctions, which is defined as $E_B = E_1 + E_2 - E_{\mathrm{vdWH}}$. Here, E_{vdWH}, E_1 and E_2 represent the total energy of the heterojunction, monoalyer $MgCl_2$ and $ZnBr_2$, respectively. Considering the negative signs of the energies, a higher (more positive) binding energy means a more strongly bounded and stable system. The AA structure is the most stable one among the three vdWHs, as indicated in Table 1. Therefore, in the following we mainly investigate electronic properties and the PGE of the AA $MgCl_2/ZnBr_2$ vdWH.

Table 1 Total energy (E_{vdWH}), binding energy (E_B), interlayer spacing d and lattice constant a for three kinds of 2D $MgCl_2/ZnBr_2$ vertical vdWHs.

Stacking	E_{vdWH} (eV)	E_B (eV)	d (Å)	a (Å)
AA	−5.976	0.222	3.221	3.761
AB	−5.969	0.214	3.410	3.761
AC	−5.920	0.166	3.666	3.761

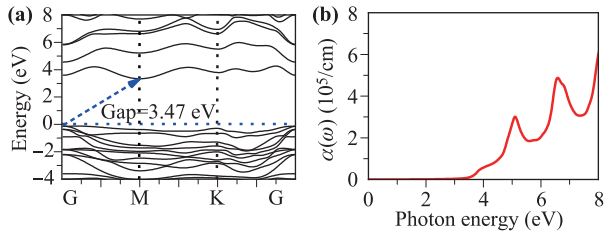

Fig. 2 **(a)** The electronic bandstructure and **(b)** optical absorption coefficient of the AA $MgCl_2/ZnBr_2$ vdWH.

The electronic bandstructure of the AA $MgCl_2/ZnBr_2$ vertical vdWH is shown in Fig. 2(a). It has an indirect bandgap of 3.47 eV, with the valence band maximum (VBM) located at Gamma point, while the conduction band minimum (CBM) is located at M point. Figure 2(b) shows the absorption coefficient $\alpha(\omega)$ of the AA $MgCl_2/ZnBr_2$ vdWH. There are two prominent absorption peaks located in the ultraviolet range, and the first peak appears at around 5.1 eV. We will focus on the PGE for the photon energy lower than 6.0 eV, which covers the first absorption peak.

We model an UV-PD by using the AA $MgCl_2/ZnBr_2$ vdWH, which contains: left and right electrodes (leads), and the central region, as indicated in Fig. 3(a). The whole device is periodical in the x-direction, and two electrodes are extended into $z = \pm\infty$, respectively. When the center region is illuminated by linearly polarized light, the PGE is generated due to the C_{3v} symmetry, giving rise

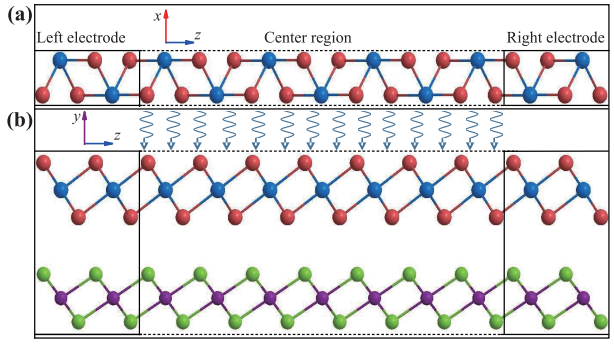

Fig. 3 Atomic model for the photodetector composed of the AA $MgCl_2/ZnBr_2$ vertical vdWH. **(a)** and **(b)** are top and side views of the photodetector, respectively. The blue curved arrows in (b) represent the vertically incident linearly polarized light on the center region.

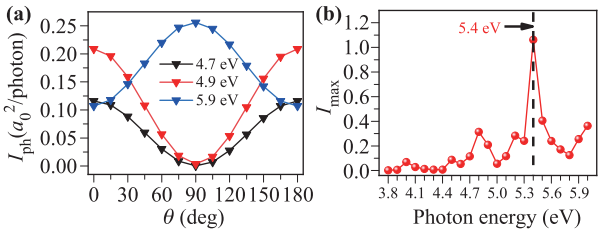

Fig. 4 **(a)** Variation of the photocurrent with the polarization angle θ for photon energies of 4.7, 4.9 and 5.9 eV. **(b)** The maximum photocurrent for different photon energies.

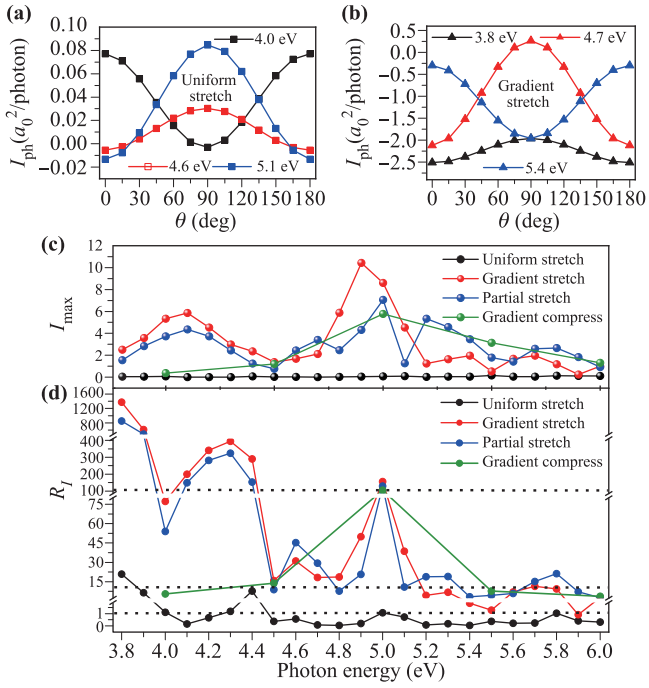

Fig. 5 Variation of the photocurrent with the polarization angle θ for **(a)** the uniform stretch and **(b)** gradient stretch. **(c)** The maximum photocurrent at different photon energies for three types of stretches. **(d)** The increase ratio R_I of the photocurrent under stretch with respect to that without the stretch.

to a robust photocurrent that flows along the z direction. The photon energy considered is from 3.5 to 6.0 eV, which is greater than the bandgap of the vdWH and covers the first optical absorption peak.

Our calculations show that the PGE photocurrent has a form $\beta \times \cos 2\theta + I_0$, which is determined by the C_{3v} symmetry, in agreement with the phenomenological theory of the PGE [35, 36]. Here, β and I_0 are determined by the symmetry and photon energy. Figure 4(a) gives the photocurrent for photon energies of 4.7 eV, 4.9 and 5.9 eV as examples, which shows an evident cosine dependence on the polarization angle θ. We can then obtain the maximum photocurrent ($I_{\max}$) at either $\theta = 0°$ or $\theta = 90°$ for each photon energy. The $I_{\max}$ for different photon energies is shown in Fig. 4(b). For photon energies of 3.5, 3.6, and 3.7 eV, the photocurrent is very small with a magnitude of 10^{-4} (not shown), and from 3.8 eV the photocurrent begins to increase. The photocurrent reaches the maximum (1.06) at 5.4 eV. Overall, the photocurrent in the higher photon energy range ($>$ 4.5 eV) is larger than that in the low photon energy range (3.5–4.5 eV), which should be partly attributed to a stronger optical absorption for high photon energies, as shown in Fig. 2(b).

Next, we investigate the influence of mechanical tension stress on the PGE photocurrent. Three types of tensile stress are exerted on the lattice. The first one is a uniform 5% stretch on the entire device along the z-direction. The second one is a partial stretch, in which only the right part of the device is stretched by 5% along the z-direction. The third is a gradient stretch: The left electrode and the left 2/7 of the center region are invariant; the following 3/7 of the center region is stretched by 3% along the z-direction; the rest 2/7 of the center region and the right electrode are stretched by 5%. For the uniform stretch, the C_{3v} symmetry of the photodetector is not changed, so that the photocurrent remains the cosine dependence on the 2θ, as shown in Fig. 5(a). For the partial and gradient stretch, the symmetry of the photodetector is reduced from the C_{3v} to C_s, while the photocurrent still holds the cosine form under the C_s symmetry, as shown in Fig. 5(b), which is in a good agreement with the phenomenological theory of the PGE. The maximum photocurrent for different photon energies is shown in Fig. 5(c). It can be seen that the photocurrent under partial and gradient stretches (the blue and red spheres) is much larger than that of the uniform stretch. Here, we calculate the increase ratio R_I of the photocurrent, which is the ratio of the photocurrent under mechanical strain with respect to that without any strain, as shown in Figs. 5(d). The maximum R_I is 1372 at 3.8 eV for the gradient stretch, and is 849 at 3.8 eV for the partial stretch. For a number of photon energies, e.g., 4.1 to 4.4 eV, R_I is greater than 100, and moreover, for all photon energies, R_I is greater than 1 for both the partial and gradient stretches. In contrast, for uniform stretch the photocurrent only increases for a few of low photon energies, and is even decreased for some high energies. These results show that the magnitude of the photocurrent can be largely enhanced by partial and gradient stretches. The reason is that the device is reduced from the C_{3v} symmetry to the C_s symmetry under partial and gradient stretches, which means that the device becomes more asymmetric, in other words, the device asymmetry is increased. The magnitude of the photocurrent has a linear dependence on the device asymmetry, as proposed in our previous work [24], and therefore, the photocurrent is largely enhanced. In contrast, for the uniform stretch the symmetry of the photodetector is not changed, so that the magnitude of the photocurrent does not change considerably.

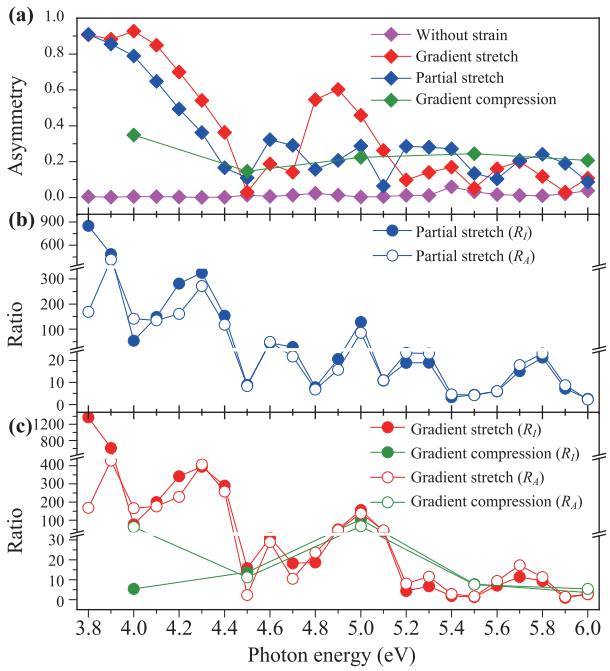

Fig. 6 **(a)** The device symmetry A at different photon energies for different mechanical strain. **(b)** Comparison of the R_I with the increase ratio of the device asymmetry (R_A) for partial stretch, and **(c)** for gradient stretch and compression.

Then, we calculate the device asymmetry A, and also the increase ratio R_A of the device asymmetry with respect to that without any strain. Figure 6(a) plots the device symmetry A at different photon energies for different mechanical strain, which shows that the device asymmetry is considerably increased, as compared to that without any strain (the pink squares). Furthermore, we compare R_I with R_A in Figs. 6(b) and (c) at different photon energies for different mechanical strain. It can be seen that the overall trend of the R_I agrees very well with that of the R_A for almost all of the photon energies. We also examined the photocurrent under gradient compression for several photon energies, and found that the photocurrent is also significantly enhanced, with a largest R_I of 128 at 5.0 eV, as shown in Figs. 5(c) and (d) (see the green circles). This is also attributed to the largely increased device asymmetry [see Figs. 6(a) and (c)]. These results strengthen that the inhomogenous strain including partial stretch, gradient stretch and gradient compression can effectively enhance the PGE photocurrent in the photodetector because of the reduced device symmetry.

4 Conclusions

In conclusion, we have studied the PGE in the photodetector composed of the 2D $MgCl_2/ZnBr_2$ vertical vdWH by using quantum transport simulations. PGE photocurrent is generated at zero bias under the illumination of linearly polarized light in the UV range for photon energies from 3.8 eV to 6.0 eV, owing to the noncentrosymmetric C_{3v} symmetry. By applying partial stretch (5%) and gradient stretch along the transport direction on the device, the PGE photocurrent is largely enhanced by up to 3 orders of magnitude for all of the photon energies. This is because the partial and gradient stretches reduce the device symmetry from the C_{3v} to the C_s, which increases the device asymmetry, and therefore the photocurrent. Our results propose an effective way to largely enhance the PGE by inhomogenous tensile stress, and suggest a potential application of the 2D $MgCl_2/ZnBr_2$ vertical vdWH in the low-power UV photodetection.

Acknowledgements This work was supported by the National Natural Science Foundation of China under Grant No. 51871156.

References

1. H. Chen, H. Liu, Z. Zhang, K. Hu, and X. Fang, Nanostructured photodetectors: From ultraviolet to terahertz, *Adv. Mater.* 28(3), 403 (2016)
2. Q. Zhang, X. Li, Z. He, M. Xu, C. Jin, and X. Zhou, 2D semiconductors towards high-performance ultraviolet photodetection, *J. Phys. D* 52(30), 303002 (2019)
3. D. Guo, Y. Su, H. Shi, P. Li, N. Zhao, J. Ye, S. Wang, A. Liu, Z. Chen, C. Li, and W. Tang, Self-powered ultraviolet photodetector with superhigh photoresponsivity (3.05 A/W) based on the GaN/Sn:Ga_2O_3 pn Junction, *ACS Nano* 12(12), 12827 (2018)
4. W. Zheng, R. Lin, Y. Zhu, Z. Zhang, X. Ji, and F. Huang, Vacuum ultraviolet photodetection in two-dimensional oxides, *ACS Appl. Mater. Interfaces* 10(24), 20696 (2018)
5. W. Zheng, R. Lin, Z. Zhang, and F. Huang, Vacuum-ultraviolet photodetection in few-layered h-BN, *ACS Appl. Mater. Interfaces* 10(32), 27116 (2018)
6. Y. Gao, S. Lei, T. Kang, L. Fei, C. L. Mak, J. Yuan, M. Zhang, S. Li, Q. Bao, Z. Zeng, Z. Wang, H. Gu, and K. Zhang, Bias-switchable negative and positive photoconductivity in 2D $FePS_3$ ultraviolet photodetectors, *Nanotechnology* 29(24), 244001 (2018)
7. H. Kan, W. Zheng, R. C. Lin, M. Li, C. Fu, H. B. Sun, M. Dong, C. H. Xu, J. T. Luo, Y. Q. Fu, and F. Huang, Ultrafast photovoltaic-type deep ultraviolet photodetectors using hybrid zero-/two-dimensional heterojunctions, *ACS Appl. Mater. Interfaces* 11(8), 8412 (2019)
8. Y. Gao, Y. Zhang, and D. Xiao, Tunable layer circular photogalvanic effect in twisted bilayers, *Phys. Rev. Lett.* 124(7), 077401 (2020)
9. R. von Baltz and W. Kraut, Theory of the bulk photovoltaic effect in pure crystals, *Phys. Rev. B* 23(10), 5590 (1981)
10. V. I. Belinicher, Space-oscillating photocurrent in crystals without symmetry center, *Phys. Lett. A* 66(3), 213 (1978)
11. S. D. Ganichev and W. Prettl, Spin photocurrents in quantum wells, *J. Phys.: Condens. Matter* 15(20), R935 (2003)

12. X. Tao, P. Jiang, H. Hao, X. Zheng, L. Zhang, and Z. Zeng, Pure spin current generation via photogalvanic effect with spatial inversion symmetry, *Phys. Rev. B* 102(8), 081402 (2020)
13. M. M. Ramin Moayed, F. Li, P. Beck, J. C. Schober, and C. Klinke, Anisotropic circular photogalvanic effect in colloidal tin sulfide nanosheets, *Nanoscale* 12(11), 6256 (2020)
14. M. Chen, K. Lee, J. Li, L. Cheng, Q. Wang, K. Cai, E. E. M. Chia, H. Chang, and H. Yang, Anisotropic picosecond spin-photocurrent from Weyl semimetal WTe_2, *ACS Nano* 14(3), 3539 (2020)
15. C. Guo, Y. Hu, G. Chen, D. Wei, L. Zhang, Z. Chen, W. Guo, H. Xu, C. N. Kuo, C. S. Lue, X. Bo, X. Wan, L. Wang, A. Politano, X. Chen, and W. Lu, Anisotropic ultrasensitive $PdTe_2$ -based phototransistor for room-temperature long-wavelength detection, *Sci. Adv.* 6(36), eabb6500 (2020)
16. Y. Luo, Y. Hu, and Y. Xie, Highly polarization-sensitive, visible-blind and self-powered ultraviolet photodetection based on two-dimensional wide bandgap semiconductors: A theoretical prediction, *J. Mater. Chem. A* 7(48), 27503 (2019)
17. Y. Peng, X. T. Liu, Z. H. Sun, C. M. Ji, L. N. Li, Z. Y. Wu, S. S. Wang, Y. P. Yao, M. C. Hong, and J. H. Luo, Exploiting the bulk photovoltaic effect in a 2D trilayered hybrid ferroelectric for highly sensitive polarized light detection, *Angew. Chem. Int. Ed.* 59(10), 3933 (2020)
18. Y. J. Zhang, T. Ideue, M. Onga, F. Qin, R. Suzuki, A. Zak, R. Tenne, J. H. Smet, and Y. Iwasa, Enhanced intrinsic photovoltaic effect in tungsten disulfide nanotubes, *Nature* 570(7761), 349 (2019)
19. J. E. Spanier, V. M. Fridkin, A. M. Rappe, A. R. Akbashev, A. Polemi, Y. Qi, Z. Gu, S. M. Young, C. J. Hawley, D. Imbrenda, G. Xiao, A. L. Bennett-Jackson, and C. L. Johnson, Power conversion efficiency exceeding the Shockley–Queisser limit in a ferroelectric insulator, *Nat. Photonics* 10(9), 611 (2016)
20. J. Li and P. M. Haney, Circular photogalvanic effect in organometal halide perovskite $CH_3NH_3PbI_3$, *Appl. Phys. Lett.* 109(19), 193903 (2016)
21. M. M. Yang, D. J. Kim, and M. Alexe, Flexo-photovoltaic effect, *Science* 360(6391), 904 (2018)
22. H. Zou, C. Zhang, H. Xue, Z. Wu, and Z. L. Wang, Boosting the solar cell efficiency by flexo-photovoltaic effect? *ACS Nano* 13(11), 12259 (2019)
23. S. Nadupalli, J. Kreisel, and T. Granzow, Increasing bulk photovoltaic current by strain tuning, *Sci. Adv.* 5(3), eaau9199 (2019)
24. J. Zhao, Y. Hu, Y. Xie, L. Zhang, and Y. Wang, Largely enhanced photogalvanic effects in a phosphorene photodetector by strain-increased device asymmetry, *Phys. Rev. Appl.* 14(6), 064003 (2020)
25. N. Mounet, M. Gibertini, P. Schwaller, D. Campi, A. Merkys, A. Marrazzo, T. Sohier, I. E. Castelli, A. Cepellotti, G. Pizzi, and N. Marzari, Two-dimensional materials from high-throughput computational exfoliation of experimentally known compounds, *Nat. Nanotechnol.* 13(3), 246 (2018)
26. G. Kresse and J. Furthmüller, Efficient iterative schemes for *ab initio* total-energy calculations using a plane-wave basis set, *Phys. Rev. B* 54(16), 11169 (1996)
27. G. Kresse and D. Joubert, From ultrasoft pseudopotentials to the projector augmented-wave method, *Phys. Rev. B* 59(3), 1758 (1999)
28. J. P. Perdew, K. Burke, and M. Ernzerhof, Generalized gradient approximation made simple, *Phys. Rev. Lett.* 77(18), 3865 (1996)
29. J. Taylor, H. Guo, and J. Wang, *Ab initio* modeling of quantum transport properties of molecular electronic devices, *Phys. Rev. B* 63(24), 245407 (2001)
30. L. E. Henrickson, Nonequilibrium photocurrent modeling in resonant tunneling photodetectors, *J. Appl. Phys.* 91(10), 6273 (2002)
31. Y. Xie, M. Chen, Z. Wu, Y. Hu, Y. Wang, J. Wang, and H. Guo, Two-dimensional photogalvanic spin-battery, *Phys. Rev. Appl.* 10(3), 034005 (2018)
32. Y. Xie, L. Zhang, Y. Zhu, L. Liu, and H. Guo, Photogalvanic effect in monolayer black phosphorus, *Nanotechnology* 26(45), 455202 (2015)
33. J. Chen, L. Zhang, L. Zhang, X. Zheng, L. Xiao, S. Jia, and J. Wang, Photogalvanic effect induced fully spin polarized current and pure spin current in zigzag SiC nanoribbons, *Phys. Chem. Chem. Phys.* 20, 26744 (2018)
34. L. Zhang, K. Gong, J. Chen, L. Liu, Y. Zhu, D. Xiao, and H. Guo, Generation and transport of valley polarized current in transition metal dichalcogenides, *Phys. Rev. B* 90, 195428 (2014)
35. V. I. Belinicher and B. I. Sturman, The photogalvanic effect in media lacking a center of symmetry, *Sov. Phys. Usp.* 23(3), 199 (1980)
36. S. D. Ganichev, H. Ketterl, W. Prettl, E. L. Ivchenko, and L. E. Vorobjev, Circular photogalvanic effect induced by monopolar spin orientation in *p*-GaAs/AlGaAs multiple-quantum wells, *Appl. Phys. Lett.* 77(20), 3146 (2000)